DETECTION OF EDDIES IN THE EASTERN GULF OF ALASKA USING TOPEX/POSEIDON ALTIMETRY

Steven D. Meyers, Sujit Basu and James J. O'Brien

CENTER FOR OCEAN-ATMOSPHERIC PREDICTION STUDIES
THE FLORIDA STATE UNIVERSITY
TALLAHASSEE, FL 32306-2840

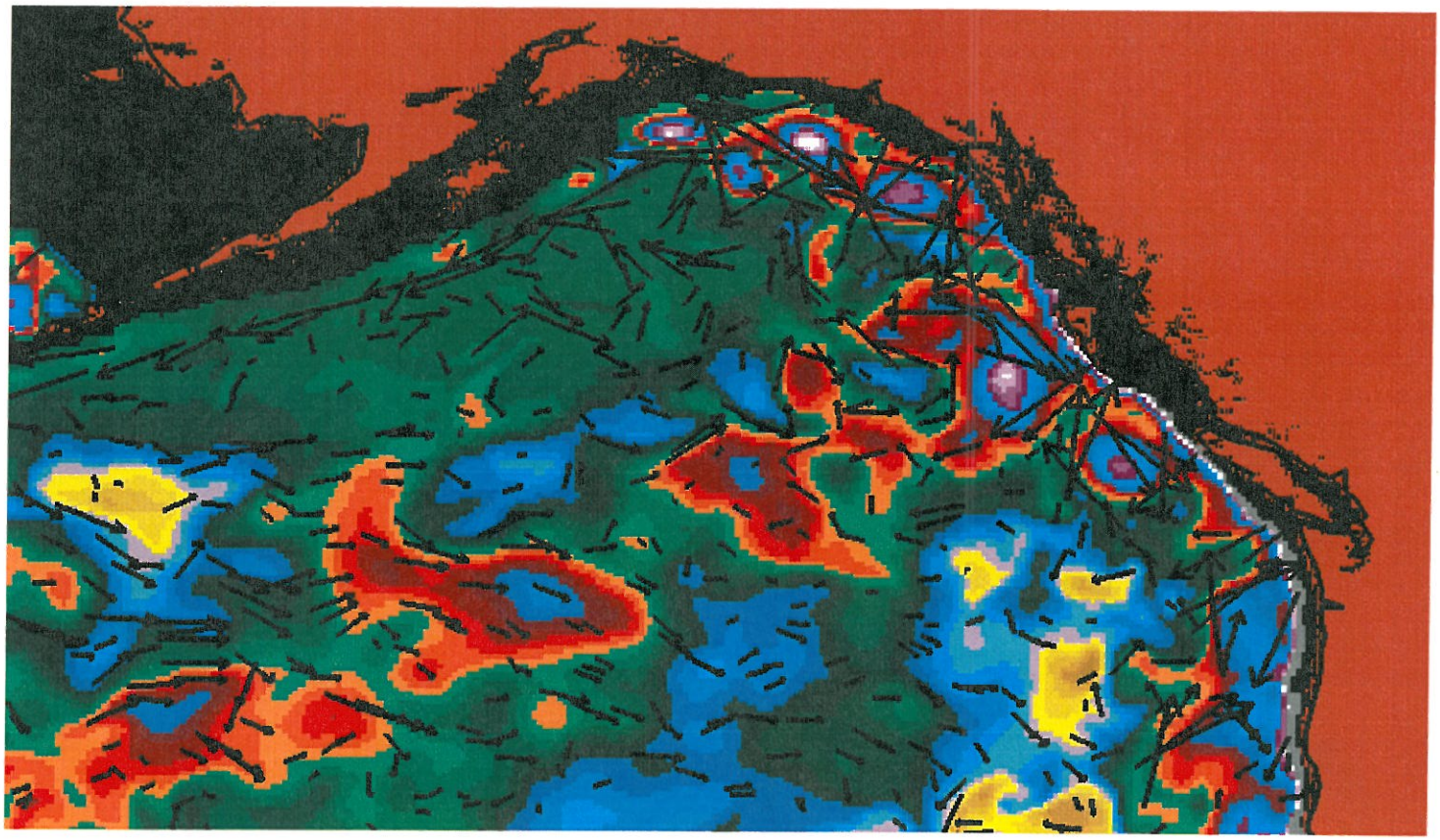

June 30, 1997
COAPS TECHNICAL REPORT 97-4

Abstract.

Along-track TOPEX altimetry is used to study eddy formation in the eastern Gulf of Alaska. The geoid and mean currents are removed from the data through extraction of the temporal and spatial averages. The resulting anomalies are passed through a matched-filter tuned to detect Gaussian signals with amplitudes ± 20 cm with widths 150 km embedded in noise.

Few eddies were found south of 50°N. Anticyclonic eddies are found to be of larger amplitude, with a larger amplitude variance, and a broader distribution in space. The cyclonic features are narrowly distributed about a single amplitude with only one excursion away from this value. This occurred in 1995 when the cyclonic features became very strong. During this time the anticyclonic features were few and weak.

Introduction

The subpolar gyre of the North Pacific (NP) is defined to the south by the North Pacific Current (NPC). As the NPC impacts the west coast of North America, it splits into the southward California Current and the Northward Alaska Current (AC). The AC is a coastal current moving from southern Canada northward along the continental margin into the Aleutian Islands. Along the Korean coast the southward Oyashio completes the cyclonic circulation of the subpolar gyre.

Other than the seasonal cycle, the largest climatic cycle affecting the NP is the El Nino/Southern Oscillation (ENSO). ENSO effects the extratropical oceans in two ways: locally, through changes in the surface winds, and, remotely, via tropically generated coastally trapped Kelvin. Numerical ocean models show that tropically generated Kelvin waves are a significant source of interannual variability in the near-shore ocean circulation along western North America [*Pares-Sierra and O'Brien*, 1989], as well as the generators of large amplitude Rossby waves in the midlatitude Pacific basin [*Johnson and O'Brien*, 1990; *Jacobs et al.*, 1994]. This process plays a major role in controlling decadal climate variability [*Meyers et al.*, 1996]. In this research program, particular attention will be paid to the new theory that ENSO, via Kelvin waves, is a mechanism driving both mesoscale activity along the coast.

The existence of seasonal and interannual variations of eddy occurrences are indicated by the compilation of observations of the "Sitka eddy" by Tabata (1982), although no definitive conclusions could be drawn due to the sparsity of observations in the area.

Eddy formation due to these waves also seems consistent with observations. In an extensive examination of oceanographic data collected during 1927-77 in the Gulf of Alaska, *Tabata* [1982] concluded that "baroclinic eddies occur frequently in this region. Among these is the recurring, well developed, anticyclonic eddy situated within a few hundred kilometers of Sitka", now commonly called the Sitka eddy. The primary characteristics of the Sitka eddy are diameter 150 km - 300 km, SSH deflection 10-20 cm, with an initial location ~200 km off Baranof Is., and a lifetime of order one year.

Previous studies have hypothesized that the interannual variability in the Gulf of Alaska may be affected by ENSO events in the tropical Pacific Ocean (Emery and Hamilton, 1985; Mysak, 1985).

Although such a link is not discussed by Tabata (1982), the observations of the Sitka eddy indicate interannual variability, yielding clues to any relationship with the tropical ocean. Tabata (1982) refers to the possible presence of the Sitka eddy with various degrees of certainty. The uncertainty may be attributed to the sparsity of available data as well as interannual variability of the mesoscale ocean circulation off Sitka.

Results from a NRL (Naval Research Laboratories, Stennis) high-resolution, isopycnal ocean model driven with realistic daily wind ECMWF fields from 1981-1993 indicated coastally trapped Kelvin waves driven by ENSO are a source of mesoscale variability along the coast [*Melsom et al.*, 1997]. Downwelling Kelvin waves can lead to strong formation of anticyclonic eddies in the Gulf of Alaska (GOA), due to an enhancement of the AC (and steepening of isopycnals) to the point of instability. Conversely, the upwelling waves associated with an ENSO cold event weakens the Alaska Current and stabilizes the coastal ocean. Strong interannual variability of the mesoscale field is thus produced by changes in the ENSO state in the NRL model.

Examination of along-track sea-level anomalies (SLA) from TOPEX-POSEIDON (TP) reveals the interannual variations in the location and intensity of the eddy behavior.

Altimeter data is inevitably noisy because of the presence of errors such as orbit error and residual errors due to atmospheric and oceanic effects. Extraction of a typical sea surface height signature due to a mesoscale eddy from this noisy data set is, therefore, a very difficult task and requires sophisticated method. In the present study we have used a technique, borrowed from signal processing literature [*Helstrom*, 1968]. This technique has earlier been used by *Basu et al.* [1993] for detecting Somali eddies.

The next section gives additional information regarding the altimetric data. The third section details the matched-filter technique used for eddy identification. This is followed by a section presenting the analysis, and the fifth section is a discussion of results.

Altimetry Data

TP is cooperative U.S.-French instrument designed to measure the sea surface topography [*Fu et al.*, 1994]. Several environmental biases must be removed from the raw measurements before an accurate picture of the ocean surface can be obtained. We examine the TP data from October 1992

to March, 1996, consisting of 136 descending passes along a single track.

The data is extracted from the Geophysical Data Records (GDRs) provided by JPL. The orbits based on the JGM-3 gravity model are used. The oscillator drift error has not been corrected. The corrections applied are: dry tropospheric path delay, wet tropospheric path delay, ionospheric path delay, inverse barometer (atmospheric pressure forcing of the ocean surface), electromagnetic bias, a solid earth tide, and an estimate of the ocean tide constructed by *LeProvost et al.* [1994].

The em-bias, wet troposphere, and ionospheric corrections have had an outlier detection run on them before being applied. The em-bias, wet troposphere, and ionosphere corrections were then smoothed along track using a boxcar filter of length 6 seconds for the em-bias and wet troposphere, but 10 seconds for the ionosphere.

The SSH for each repeat pass are then interpolated along track to a set of points spaced by 1 second along the T/P ground track. These points were determined by the Colorado Center for Astrodynamics Research at CU, Boulder. Thus a time series at each point along the ground tracks is constructed. Small gaps in each record are filled using temporal cubic splines.

The ascending and descending tracks in the northeast Pacific Ocean (NEP) is shown in Fig. 1. Only a single track is close and parallel to the eastern GOA without intersecting many islands. This track is the only one selected for examination.

Eddy Detection

The approach is based on matched filter technique for detecting a given signal in a noisy data. The technique consists of the following three steps. *i*) Estimation of the noise power spectral density (PSD) of this track. For this purpose each track is represented by an autoregressive model of finite order, i.e., the time series of sea level anomaly $\{z(t), t = 1, 2, ..., n\}$ is written as:

$$z(t) = \sum_{i=1}^{p} C_i z(t-i) + W_p(t), t = p+1, ..., n \tag{1}$$

where $W_p(t)$ is zero mean white noise of variance σ_p^2. and $C_1, ..., C_p$ are the autoregressive coefficients. The standard autoregressive problem is solved. This estimates the order p best supported by the data and the AR parameters $\{C_i\}$ and σ_p^2, given the data $\{z(t)\}$ and the maximum order p_{max}. The problem is solved by the modified covariance approach [*Kay*, 1988]. This approach consists of

minimizing (for each order $p = 0, 1, 2, ..., p_{max}$) the average of the estimated forward and backward prediction square error

$$\sigma_p^2 = \frac{1}{2}\left(\rho^f + \rho^b\right) \tag{2}$$

$$\rho^f = \frac{1}{n - p_{max}} \sum_{j=p_{max}+1}^{n} \left[z(j) - \sum_{i=1}^{p} C_i z(j-i) \right]^2 \tag{3}$$

$$\rho^f = \frac{1}{n - p_{max}} \sum_{j=1}^{n-p_{max}} \left[z(j) - \sum_{i=1}^{p} C_i z(j+i) \right]^2 \tag{4}$$

where $p = 0, 1, 2, ..., p_{max}$.

Minimization is done with respect to the coefficients $\{C_i\}$ and the resulting equations are solved by Cholesky decomposition technique [*Kay*, 1988]. After substituting for the estimated coefficients, Eqs (2–4) give the estimate of the white-noise variance. This estimate is then used to compute Akaike Information Criterion [*Akaike*, 1974] for each p

$$A(p) = n \ln[\sigma_p^2] + 2p \tag{5}$$

The particular p that minimizes $A(p)$ is identified: the corresponding AR parameters then define the particular AR model which is best supported by the available data. Once the coefficients $\{C_i\}$ and the white-noise variance σ^2 are known, where σ^2 is the variance for the optimal p, one can immediately find the power spectral density (PSD) of the underlying noise process analytically by the formula [*Gairola et al.*, 1992; *Basu et al.*, 1994].

$$S(f) = \frac{\sigma^2}{G(f)G(-f)} \tag{6}$$

$$G(f) = 1 - \sum_{i=1}^{p} C_i \exp(-i2\pi f i) \tag{7}$$

(*ii*) The second step involves the designing of the matched filter, which is an algorithm, optimum in terms of detecting a given signal signature in noisy data [*Gairola et al.*, 1992; *Basu et al.*, 1994]. Once the signature and the noise PSD are known, the transfer function of the filter can be written as:

$$H(f) = M(-f)/S(f) \tag{8}$$

where $M(f)$ is the signature Fourier transform, and $S(f)$ is the PSD given by (6). In the present case, the signal is the generic signature due to either anticyclonic or cyclonic eddy. This signature is

modelled as in *Basu et al.* [1993]:

$$m(x) = D \exp[-9.21(x/W)^2] \tag{9}$$

where x = distance along satellite ground track, D = maximum signature height, and W = signature width. Here D may be either positive or negative, depending on whether the eddy is cyclonic or anticyclonic, respectively. Conversion from spatial to temporal domain and vice versa is easily accomplished using the velocity of the sub-satellite point (c =5.94 km/s for TP) as $x = ct$. The values used are $D = 0.2$ m for anticyclonic and $D = -0.2$ m for cyclonic eddies, and $W = 150$ m. These are typical values for eddies occurring in the Alaska region, the region of study.

The impulse response of the matched filter is obtained by inverse Fourier transform. Processing the data series by this matched filter is equivalent to taking the convolution

$$y(t) = \sum_{i=-\infty}^{+\infty} h(i) z(t-i) \tag{10}$$

where $h(i)$ denotes the impulse response of the matched filter

$$h(i) = \sigma^{-2} g(i) * [g(-i) * m(-i)] \tag{11}$$

Here the asterisk denotes convolution. $g(t)$ and $h(t)$ are the inverse Fourier transforms of $G(f)$ and $H(f)$, respectively, which can be evaluated analytically and $m(t)$ is the signal in the time domain. The output of the filter is scaled by the rms signal-to-noise ratio SNR, i.e.,

$$Y(t) = y(t)/SNR \tag{12}$$

where

$$SNR = \left[\sum_{i=-\infty}^{+\infty} h(i) m(-i) \right]^{1/2} \tag{13}$$

This scaling ensures that the output contains a random component having standard deviation of unity. The sums in (10) and (13) will contain only a finite number of terms because of the finite support property of the signal and of the filter impulse response.

(*iii*) The final step consists of applying a threshold detector. The output $Y(t)$ is compared with a predetermined threshold (TH), chosen to produce a specified false alarm rate (FAR)

$$TH = \left[2 \ln \left(\frac{F_m}{FAR} \right) \right]^{1/2} \tag{14}$$

Here F_m is the rms bandwidth of the filter output,

$$F_m = \frac{1}{2\pi} \cos^{-1}\left(\frac{X}{SNR^2}\right) \tag{15}$$

where

$$X = \sum_{i=-\infty}^{+\infty} h(i)m(1-i) \tag{16}$$

The maximum-likelihood estimate of the location of the detected eddy signature is the value of t for which Y(t) achieves a local maximum above the threshold TH. The amplitude of the detected signature is

$$A = DY(t_0)/SNR \tag{17}$$

where $Y(t_0)$ denotes the scales output at the detected location t_0.

The algorithm is very efficient, completing the eddy detection over 136 tracks in less than one second on a SGI workstation. This completes the description of the methodology of the matched filter technique.

Results

The sea level with reference to the ellipsoid has about a 50 m variation over the eastern GOA (Fig. 2). Relatively small variations can be seen in the field, such as along 51°N. The data dropouts are filled using cubic splines in time. The mean value of the SL at each point along the track is removed. This eliminates the geoid as well as the signature of the mean ocean circulation. Time-dependent biases are removed by then subtracting the along-track mean for every pass. Eddies dominate the resulting sea level anomaly (SLA).

SL anomalies

The SLA on November 4, 1993 for the highlighted track in Fig. 1 is shown in Fig. 3a. A single anticyclonic eddy is detected near 56.5°N with amplitude $\sim$ 18 cm. The positive anomalies between 45 and 50°N do not meet the threshold requirements due to their narrow breadth and asymmetric structure. On this same date, a cyclonic eddy is found just north of the large anticyclonic eddy (Fig. 4b). The amplitude of this eddy is about 12 cm. A second eddy with amplitude about 8 cm is found near 51.7°N. The horizontal dashed line in this and subsequent figures indicates the detection

threshold corresponding to a chosen false alarm rate (FAR) of 1.0 alarms/megameter. The filter output has been truncated at the ends to avoid edge effects arising out of numerical convolution. The number of points to be deleted at both the ends vary from case to case and is decided by the algorithm itself.

Two months later on Jan 3, 1994 (Fig. 5), a large positive feature, $\sim$ 18 cm and roughly symmetric about the peak, is again seen near 57°N. The other strong positive features again do not meet the requirements to be selected as eddies. The 18 cm feature near 58°N is not selected, probably because of its narrow, double-peaked structure. No cyclonic eddy is detected along this same track north of the large anticylonic eddy (Fig. 6).

The timing, distribution, and evolution of these eddies during the time examined are now presented.

Eddy statistics

Fig. 7 shows the evolution of the SLA in the eastern GOA. A dynamical boundary is apparent around 50°N. To the south the SLA is predominantly the seasonal cycle and a roughly 60 day oscillation which appears in all the other tracks we examined (not shown) and is probably tidal in nature. Many positive and negative SLA features are apparent. Most of the negative features are relative broad, typically 1–2° in latitudinal extent with amplitude around 10. The major positive features are more localized, $\lesssim 1°$ with amplitudes 15–20 cm.

The SLAs in the eastern GOA have a range of roughly $\pm$20 cm, with most of the strong activity occurring north of 50°N. The anticyclonic eddies selected by the matched filter have a broad distribution of amplitudes from 7-25 cm (Fig. 8a) with the strongest weighting near 10 cm. Several eddies are found >25 cm. In contrast, the cyclonic eddies are relatively symmetrically distributed about 10$\pm$5 cm as seen in Fig. 9a. Very few cyclonic eddies have amplitude 15-20 cm and only a couple are found >20 cm.

Anticyclonic eddies are found fairly evenly from 50-60°N. Only a few are found south of 50°N. The cyclonic eddies are not as evenly distributed and appear to have a distribution peak near 56°N and a secondary peak near 51°N. See Fig. 10.

The temporal evolution of the eddy field (Fig. 10) indicates variations in the eddy occurence.

Most notable is the decline in anticyclonic activity in 1995 and the simultaneous increase in cyclonic activity. The difference between anticyclonic and cyclonic mean amplitudes and variance is apparent.

Discussion

Sea level data from the TOPEX/POSEIDON altimeter are used to examine eddy formation in the eastern GOA. A single track parallel to the coast, with few dropouts and little interference by land is selected. First the temporal mean at each point is subtracted, removing the geoid and mean currents. The spatial mean was then removed at each time to aid eddy detection.

Anticyclonic and cyclonic eddies were sought using a matched filter technique discussed above. The results suggest a dynamical boundary near 50°N, south of which there is little eddy activity. Anticyclonic eddies are generally stronger in amplitude and have a broader distribution of amplitudes than cyclonic eddies. The occurence of strong cyclonic eddies appears to be anticorrelated to the existence of strong anticyclonic eddies.

Most of the strong positive anomalies are associated with eddies, based on their size, shape and strength. The largest negative anomaly, in 1995, was not identified as an eddy during most of its lifetime, probably due to its large spatial extent (Fig. 11).

Numerical ocean models have indicated a relation between the state of the El Nino/Southern Oscillation (ENSO) and eddy formation in the eastern GOA. El Nino events were determined by *Melsom et al.* [1997] to destabilize the Alaska Current and produce a change of strong anticyclonic eddies along the eastern GOA which slowly migrate westward and live for over one year. The mechanism in that manuscript was the coastally trapped Kelvin wave generated in the tropics. It takes roughly 2 months for this wave to propagate from the equator to the GOA and another couple months for the eddies to develop. ENSO cold events (El Viejo, La Nina) were determined to stabilize the current system and suppress eddy formation.

During the time of the TP data examined here, 2 ENSO warm events (1993, 1994/95) and one ENSO cold event (1995/96) occurred. This would imply more anticyclonic activity in 1993-1995 and reduced activity in 1996. However, anticyclonic eddies are not reduced in 1996, but are reduced in 1995. The 1996 anticyclonic amplitudes are somewhat higher than the previous years. *Matthews et al.* [1992] examined GEOSAT SLA along a similar path and found a lack of positive SLA following

the 1988/89 ENSO cold event.

The track selected may be too far from the coast to capture the ENSO-induced eddy activity. The eddies described by *Melsom et al.* [1997] propagate slowly at $\lesssim 1$ cm/s. If these eddies have diameters of 150 km and the path is about 300 km offshore, then it will take about 6 months for the edge of the eddy to cross the TP path. The eddy will remain on the path for roughly the same amount of time.

Acknowledgements This work was supported by the Office of Naval Research, Secretary of the Navy Grant Number N00014-1-0369 which provides the base support for the research conducted by Professor James J. O'Brien, Director, The Center for Ocean-Atmospheric Prediction Studies, at The Florida State University. In addition support was received from NASA Headquarters, NASA Grant Number NA46GP0114.

Dr. Sujit Basu, on leave from the Space Applications Centre (Indian Space Research Organization) in Ahmedabad, India is working with Dr. Steven Meyers, Research Associate, COAPS, Florida State University. We wish to thank Dr. Gregg Jacobs for providing the processed altimetry data. We also want to thank Dr. James J. O'Brien, Dir., COAPS, and the personnel at COAPS for their assistance in the publication of the technical report.

List of Figures

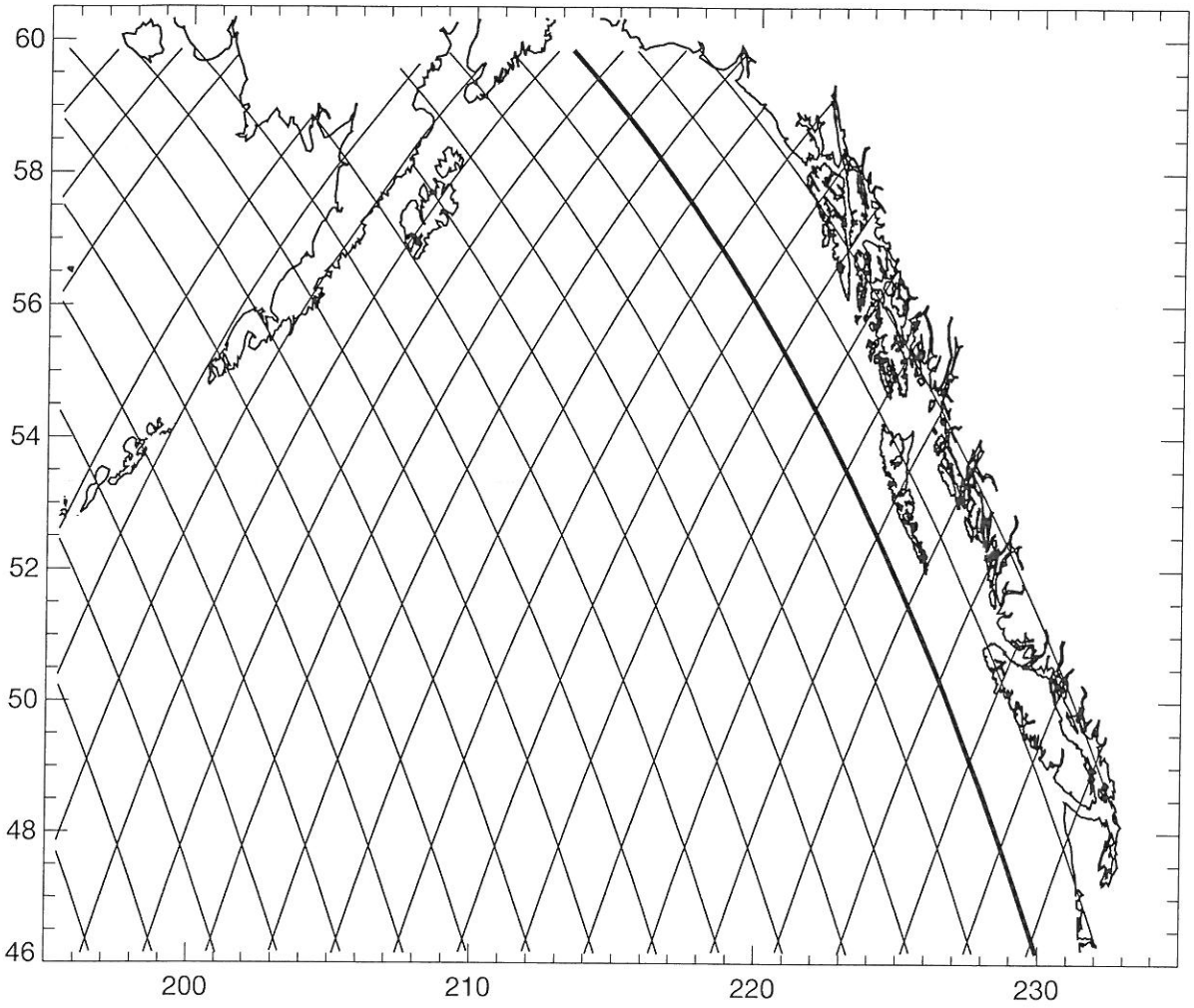

Figure 1. The tracks of TOPEX/POSEIDON in the NEP and GOA. The track with heavy line is the one examined.

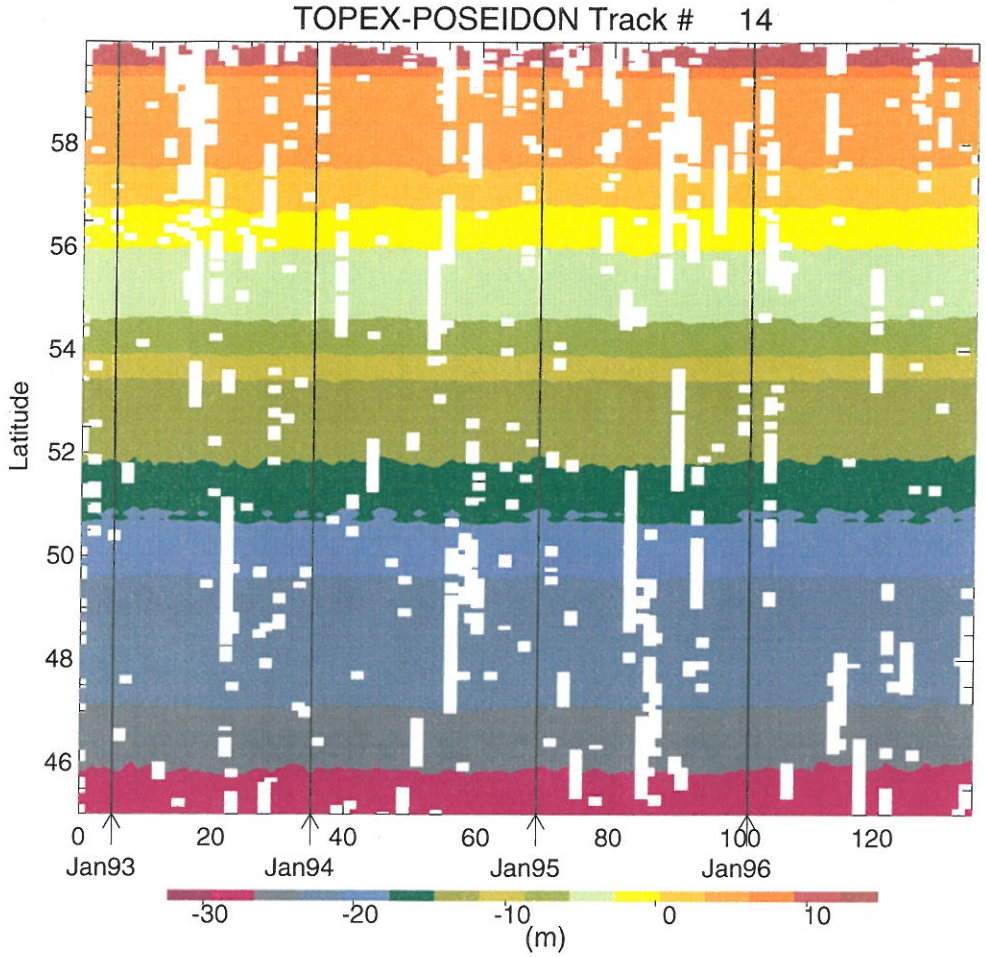

Figure 2. The TP-derived SL variation along track 14. The colors represent deviation from the ellipsoid and data dropouts are white.

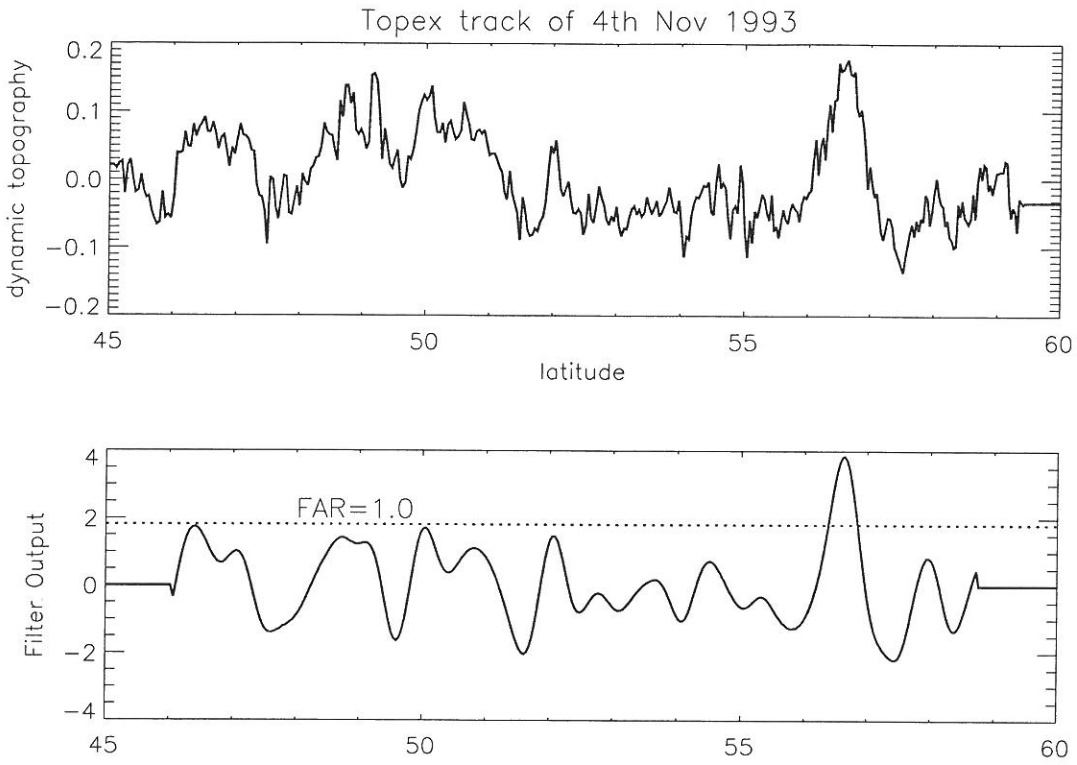

Figure 3. a) The SLA along the highlighted track in Fig. 1 on November 4, 1993. Units are meters. b) the result of the filter tuned for anticyclonic eddies with amplitude near 20 cm and widths near 150 km. The detection threshold has been indicated by the dashed line. The corresponding false alarm rate (FAR) in this and subsequent figures is measured in alarms/megameter. The trunction of the output at the ends is to avoid edge effects due to convolution.

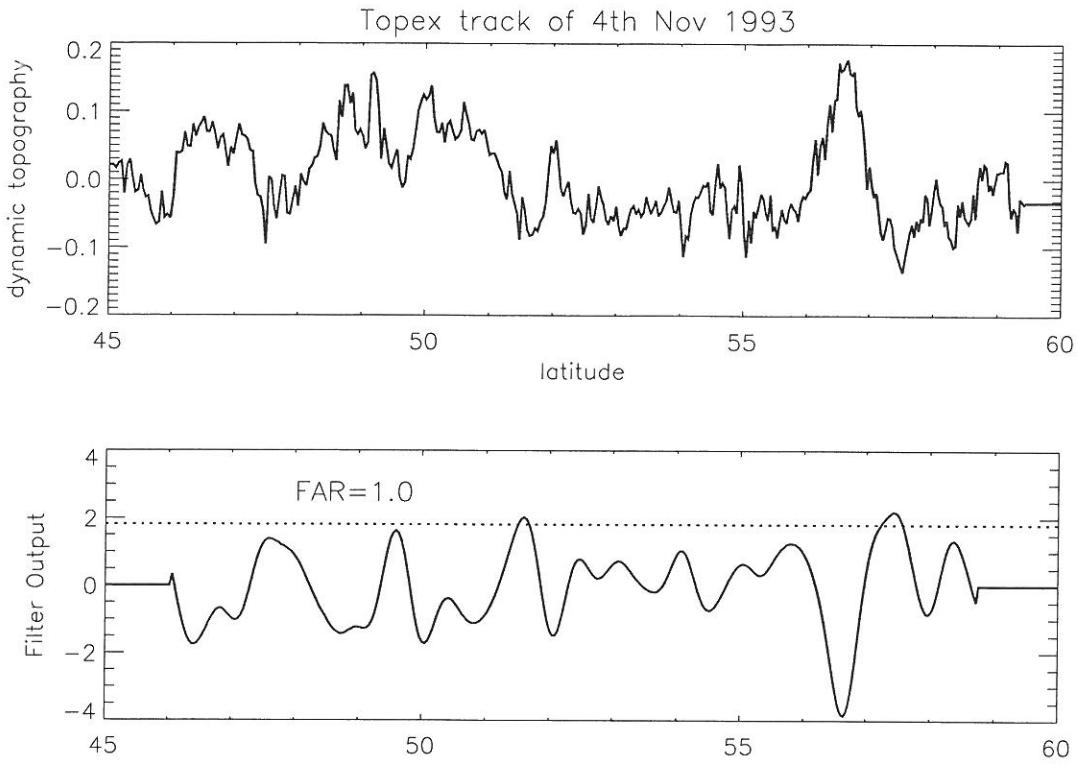

Figure 4. Same as Fig. 3, but cyclonic eddy detection.

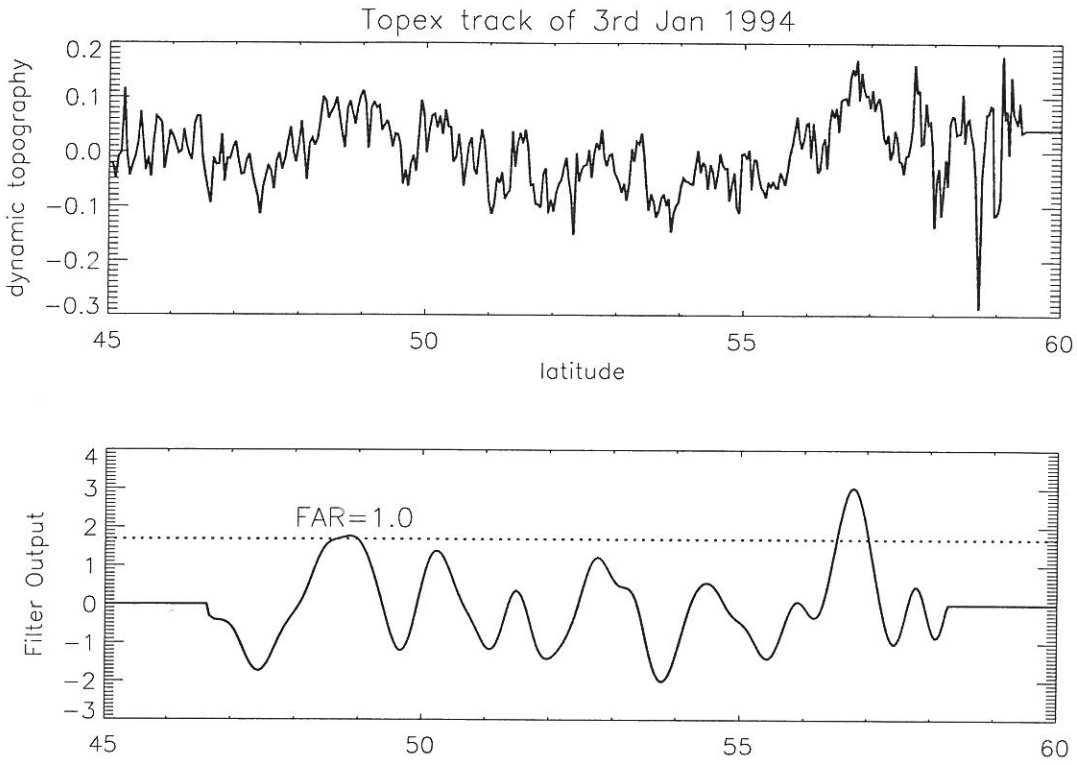

Figure 5. Same as Fig. 3, but for January 3, 1994.

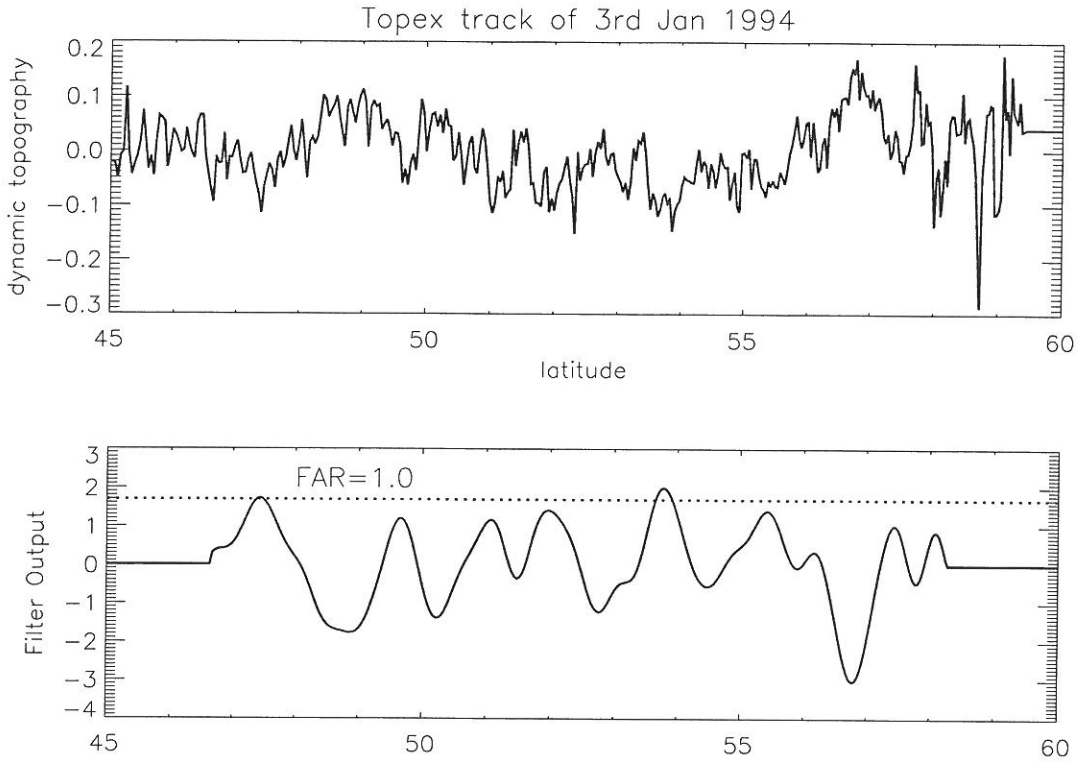

Figure 6. Same as Fig. 4, but for January 3, 1994.

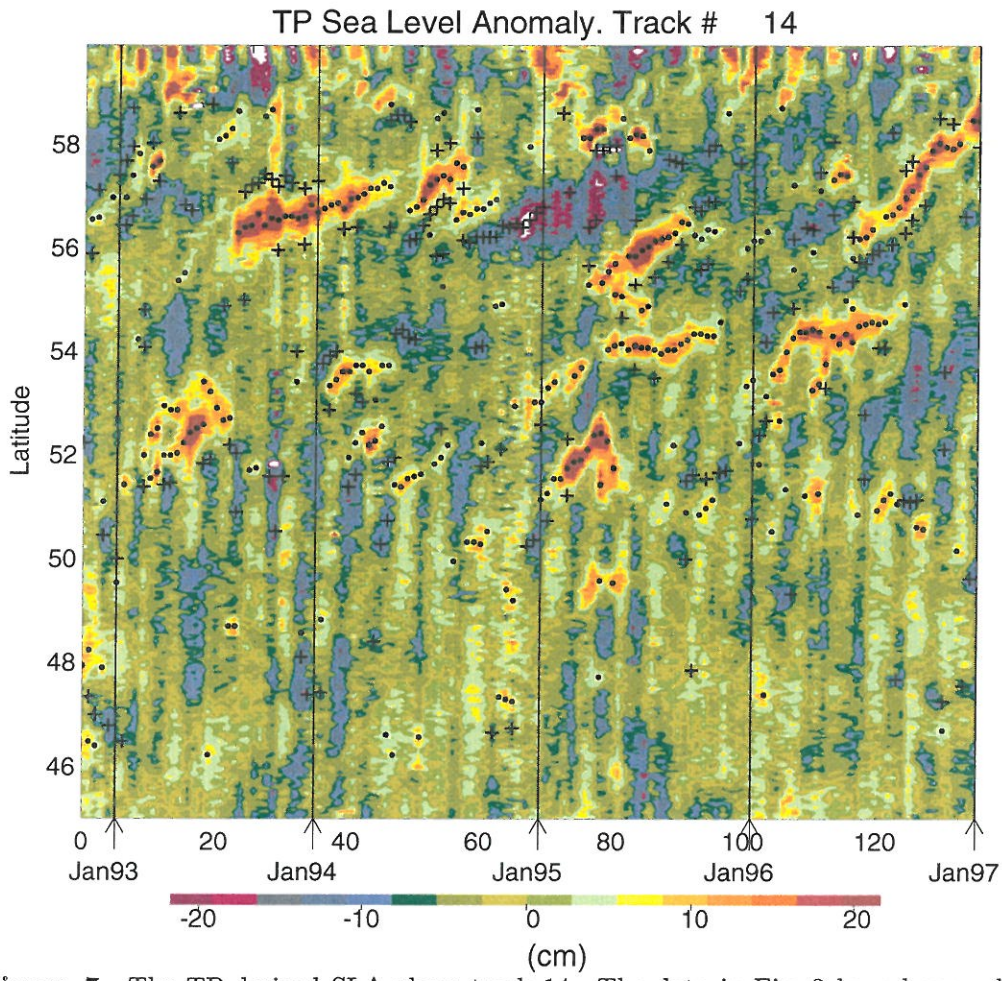

Figure 7. The TP-derived SLA along track 14. The data in Fig. 2 have been splined, the temporal and spatial means has been removed. The circles indicate locations of anticyclonic eddies and the pluses indicate cyclonic eddies, both detected using the matched-filter technique described in the text.

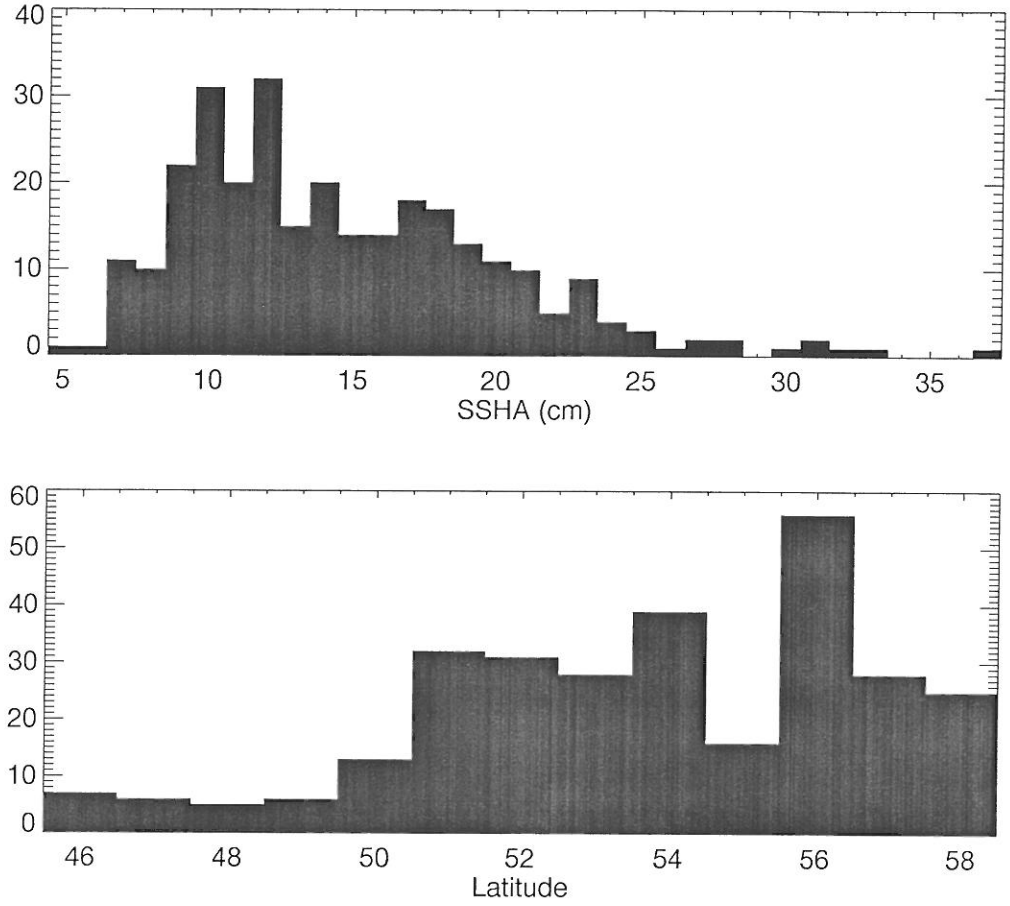

Figure 8. Statistics of the anticyclonic eddies detected by the matched-filter applied to the tracks in Fig. 7. a) Histogram of eddy amplitude. b) Histogram of eddy latitudes.

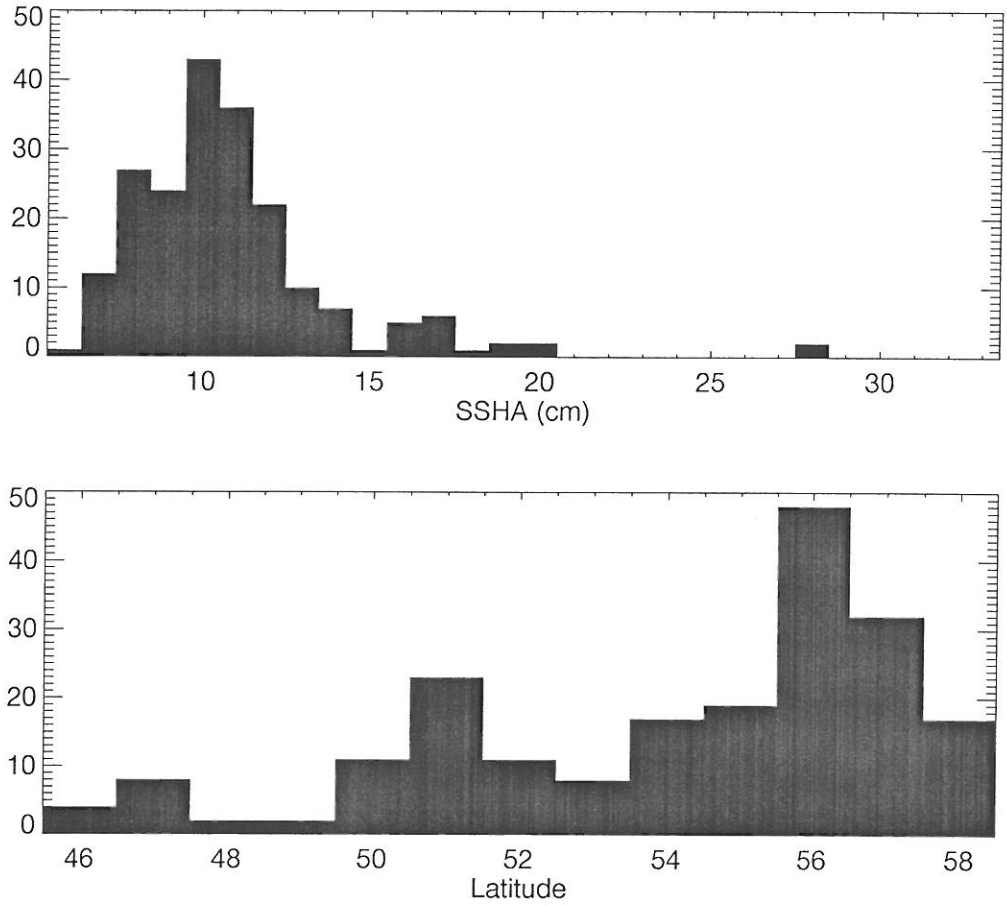

Figure 9. Statistics of the cyclonic eddies indicated in Fig. 7. a) Histogram of eddy amplitude. b) Histogram of eddy latitudes.

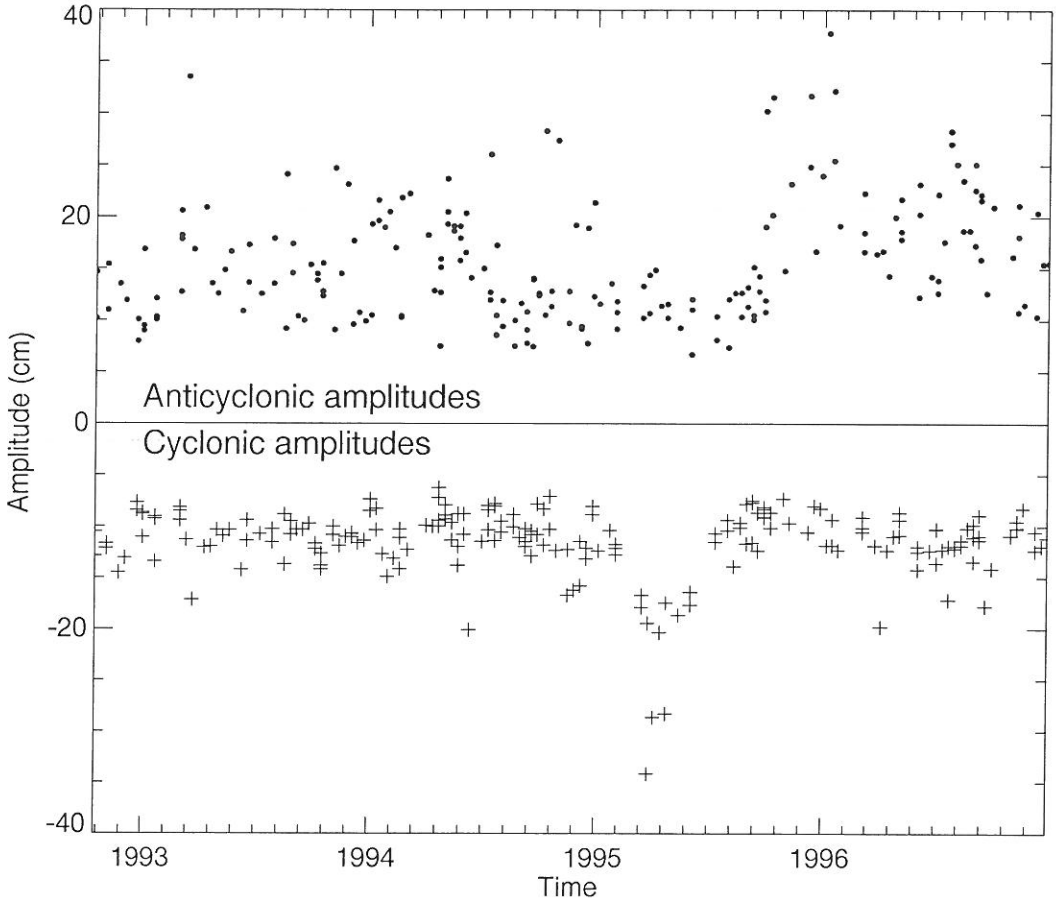

Figure 10. The amplitudes of the detected eddies from the TOPEX SLA. The circles are the amplitudes of the anticyclonic eddies. The pluses are the amplitudes of the cyclonic eddies.

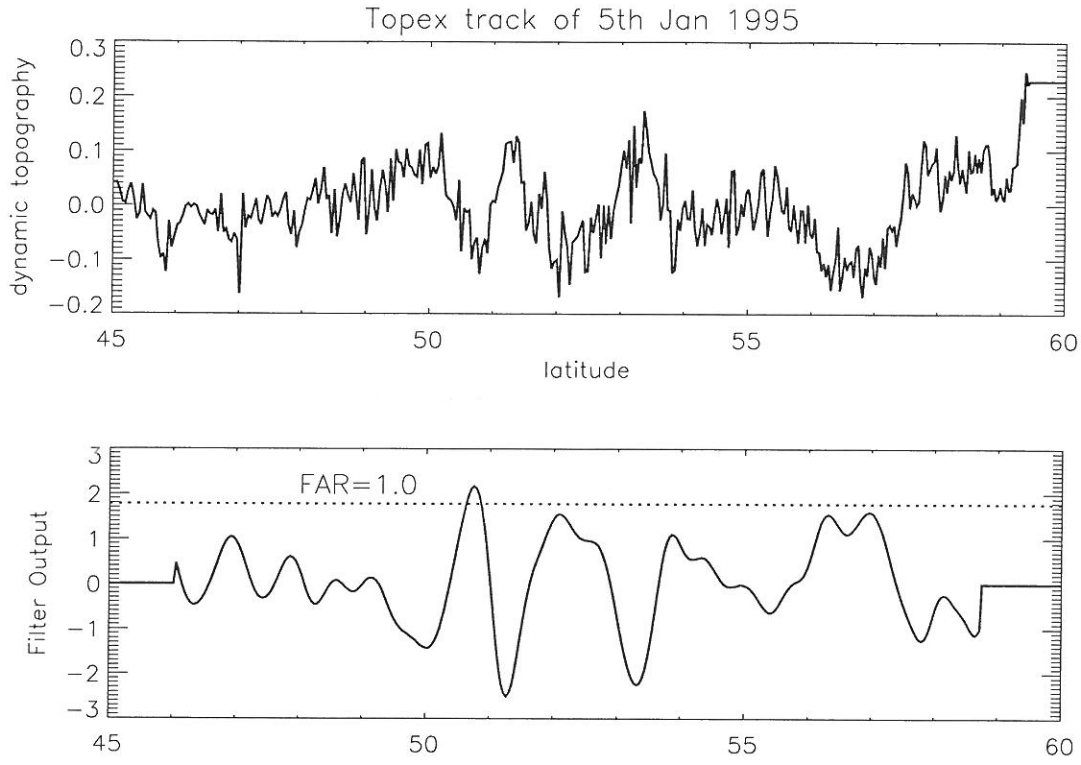

Figure 11. Same as Fig. 4, but for January 5, 1995.

References

Akaike, H., A new look at the statistical model identification, *IEEE Trans. Automat. Contr., AC-19*, 716–723, 1974.

Basu, S., R. M. Gairola, A. K. Varma, N. Gautam, and P. C. Pandey, Satellite altimetric detection of Somali eddies by signal processign technique, *Ind. J. Mar. Sci., 22*, 188–193, 1993.

Basu, S., R. M. Gairola, and P. C. Pandey, Remote sensing of seamounts in the Central Indian Ocean basin using satellite altimetry, *Rem. Sens. Rev., 9*, 187–202, 1994.

Fu, L. L., E. J. Christensen, C. A. Y. Jr., M. Lefebvre, Y. Menard, M. Correr, and P. Escudier, TOPEX/POSEIDON mission overview, *J. Geophy. Res., 99C*, 24,369–24,381, 1994.

Gairola, R. M., S. Basu, and P. C. Pandey, A Geosat-derived noise spectrum for detecting seamounts in the Arabian Sea, *Int. J. Rem. Sens., 13*, 971–979, 1992.

Helstrom, C. V., *Statistical theory of signal detection*, Pergamon Press, New York, 1968.

Jacobs, G. A., H. E. Hurlburt, J. C. Kindle, E. J. Metzger, J. L. Mitchell, W. J. Teague, and A. J. Wallcraft, Decade-scale trans-Pacific propagation and warming effects of an El Nino anomaly, *Nature, 370*, 360–363, 1994.

Johnson, M. A., and J. J. O'Brien, The northeast Pacific Ocean response to the 1982-1983 El Nino, *J. Geophy. Res., 95C*, 7,155–7,166, 1990.

Kay, S. M., *Modern spectrum analysis: theory and applications*, Prentic Hall, New Jersey, 1988.

LeProvost, C., M. L. Genco, F. Lyard, P. Vincent, and P. Canceil, Spectroscopy of the world ocean tides from a finite element hydrodynamic model, *J. Geophy. Res., 99C*, 24,777–24,798, 1994.

Matthews, P. E., M. A. Johnson, and J. J. O'Brien, Observation of mesoscale ocean features in the Northeast Pacific using Geosat radar altimetry data, *J. Geophy. Res., 97C*, 17829–17840, 1992.

Melsom, A., S. D. Meyers, H. E. Hurlburt, E. J. Metzger, and J. J. O'Brien, El Nino induced ocean eddies in the Gulf of Alaska, in preparation, 1997.

Meyers, S. D., M. Johnson, M. Liu, J. O'Brien, and J. L. Spiesberger, Interdecadal variability in a numerical model of the northeast Pacific Ocean. 1970-1989, *J. Phys. Oceanogr.*, *26*, 2,635–2,652, 1996.

Pares-Sierra, A., and J. J. O'Brien, The seasonal and interannual variability of the California current system: A numerical model, *J. Geophy. Res.*, *94C*, 3,159–3,180, 1989.

Tabata, S., The anticyclonic, baroclinic eddy off Sitka, Alaska, in the Northeast Pacific Ocean, *J. Phys. Oceanogr.*, *12*, 1260–1282, 1982.